Dual-band fiber-chip grating coupler in a 300 mm silicon-on-insulator platform and 193-nm deep-UV lithography

David González-Andrade,[1,*] Diego Pérez-Galacho,[2] Miguel Montesinos-Ballester,[3] Xavier Le Roux,[3] Eric Cassan,[3] Delphine Marris-Morini,[3] Pavel Cheben,[4,5] Nathalie Vulliet,[6] Stephane Monfray,[6] Frédéric Boeuf,[6] Laurent Vivien,[3] Aitor V. Velasco,[1] and Carlos Alonso-Ramos[3]

[1]*Instituto de Óptica Daza de Valdés, Consejo Superior de Investigaciones Científicas (CSIC), Madrid 28006, Spain*
[2]*ITEAM Research Institute, Universitat Politècnica de València, Camino de Vera s/n, 46022 Valencia, Spain*
[3]*Centre de Nanosciences et de Nanotechnologies, CNRS, Université Paris-Sud, Université Paris-Saclay, Palaiseau 91120, France*
[4]*National Research Council Canada, 1200 Montreal Road, Bldg. M50, Ottawa, Ontario K1A 0R6, Canada*
[5]*Center for Research in Photonics, University of Ottawa, Ottawa, Ontario K1N 6N5, Canada*
[6]*STMicroelectronics SAS, 850 rue Jean Monnet, 38920 Crolles, France*
**Corresponding author: david.gonzalez@csic.es*

Received XX Month XXXX; revised XX Month, XXXX; accepted XX Month XXXX; posted XX Month XXXX (Doc. ID XXXXX); published XX Month XXXX

Surface grating couplers are fundamental building blocks for coupling the light between optical fibers and integrated photonic devices. However, the operational bandwidth of conventional grating couplers is intrinsically limited by their wavelength-dependent radiation angle. Only a few dual-band grating couplers have been experimentally demonstrated, yet they exhibit low coupling efficiencies and rely on complex fabrication processes. Here we demonstrate for the first time, to the best of our knowledge, the realization of an efficient dual-band grating coupler fabricated using 193-nm deep-ultraviolet lithography for 10 Gbit symmetric passive optical networks. The footprint of the device is 17×10 μm². We measured coupling efficiencies of -4.9 dB and -5.2 dB with a 3-dB bandwidth of 27 nm and 56 nm at the wavelengths of 1270 nm and 1577 nm, corresponding to the upstream and downstream channels, respectively. © 2020 Optical Society of America

http://dx.doi.org/10.1364/OL.99.099999

The silicon-on-insulator (SOI) platform leverages microelectronics fabrication processes to achieve cost-effective mass-scale production of high-performance photonic circuits [1]. However, the tight modal confinement in SOI waveguides results in a large mode size mismatch with standard single-mode optical fibers that seriously hampers the efficiency of fiber-chip light coupling [2,3]. Surface grating couplers have been widely used for this purpose. These couplers rely on diffractive structures that can be positioned anywhere on the chip surface, allowing wafer-scale testing, and circumventing the need for optical facet preparation. Compared to edge couplers, surface grating couplers also provide an easier alignment process along with more relaxed tolerances to fabrication deviations [4]. Nevertheless, the operation of conventional grating couplers relies on radiation of a single beam at a given angle to couple the light between the chip and the optical fiber, which generally limits operation to wavelength ranges on the order of a few tens of nanometers. This restriction inherently arises from the phase-matching condition relating radiation angle, wavelength and refractive index [5,6]. While broadband grating couplers can yield a bandwidth of ~100 - 150 nm [7,8], this is still insufficient for emerging applications like next-generation passive optical networks (PON) [9]. By way of illustration, 10 Gbit symmetric PONs (XGS-PON) utilize upstream and downstream channels that are 307 nm apart ($\lambda_1 = 1270$ nm and $\lambda_2 = 1577$ nm) [10]. Although these access network applications have been successfully deployed using bulk optics components, silicon photonics has been identified as an enabling technology to further improve the performance in terms of bandwidth, power consumption and cost [11-13]. Efficient fiber-chip couplers operating at distinct wavelength bands are therefore key components to combine or split different optical bands.

Dual-band grating couplers working as wavelength multiplexer or demultiplexer (mux/demux) in the SOI platform were initially proposed by Roelkens *et al.* [14,15] and have since attracted growing attention for coupling and splitting optical signals at

Table 1. Experimental coupling efficiency (CE) and operating wavelengths (λ) of demonstrated dual-band grating couplers[a]

Refs.	λ_1 (nm)	CE_1 (dB)	λ_2 (nm)	CE_2 (dB)	TE/TM
[15]	1300.0	-6.0	1520.0	-4.0	TE
[16]	1485.0	-6.5	1530.0	-6.0	TE
[21]	1310.0	-8.2	1550.0	-7.1	TE&TM
[22]	1486.0	-7.4	1594.5	-7.0	TE
[22]	1481.5	-8.4	1661.5	-7.6	TE
[23]	1289.0	-7.3	1551.0	-8.2	TE
[25]	1560.0	-7.0	2255.0	-5.9	TE
[25]	1487.0	-6.9	2331.0	-5.7	TE
This work	1270.0	-4.9	1577.0	-5.2	TE

[a]The worst CE was considered in polarization-independent devices.

different wavelength bands. Leveraging this concept, and using an index matching fluid to mitigate reflections, a 1D dual-band coupler was demonstrated in [15] with coupling efficiencies better than -7 dB and -8 dB at 1310 nm and 1550 nm wavelengths, respectively. A dual-wavelength 2D grating coupler with coupling efficiencies of -6.5 dB and -6 dB at the wavelengths of 1490 nm and 1530 nm, respectively, was also demonstrated [16]. Wavelength demultiplexing couplers operating at normal incidence have been reported using different design strategies, including inverse design [17], gradient-based optimization algorithm [18] and finite-difference time-domain (FDTD) methods [19]. The latter employs a gold mirror formed underneath the structure to increase the coupling efficiency, but this requires additional (not CMOS compatible) steps during fabrication process. A novel subwavelength engineered dual-band grating coupler was recently proposed [20], exhibiting a calculated polarization-independent behavior with coupling efficiencies near -4.5 dB. Finally, couplers have also been developed that operate at different wavelength bands but without multiplexing/demultiplexing the optical signals [21-25]. Table 1 summarizes the performance of state-of-the-art dual-band grating couplers that have been experimentally demonstrated. Most of these devices have been fabricated using electron beam lithography and not yet demonstrated with 193-nm deep-ultraviolet (deep-UV) photolithography. Furthermore, some of them imply increased complexity (e.g. using index matching fluid [15] or requiring small feature sizes around 60 nm [22] and 80 nm [25]), and no grating coupler has yet been reported operating according to the ITU-PON wavelength roadmap [10]. Therefore, our results open promising prospects for the implementation of efficient and low-cost fiber-chip coupling interfaces for access network applications.

In this Letter, we propose and experimentally demonstrate an efficient dual-band grating coupler, which operates as a wavelength mux/demux in the O and C+L telecom bands in compliance with the XGS-PON wavelengths. The 1D grating section of our device is engineered to achieve opposite radiation angles, and thus combine or separate two optical signals at $\lambda_1 = 1270$ nm and $\lambda_2 = 1577$ nm wavelengths. Additionally, the material platform was optimized as a tradeoff between the waveguide propagation loss and the substrate reflectivity for higher coupler efficiency. The fabrication of our device, with a minimum feature size of 225 nm, was performed using 193-nm deep-UV process on 300-mm SOI platform [26], compatible with large-volume production.

A 3D schematic representation of the coupler is shown in Fig. 1(a). We use an SOI platform with thicknesses of $T_{Si} = 310$ nm for the Si waveguides and $T_{BOX} = 720$ nm for the buried oxide (BOX)

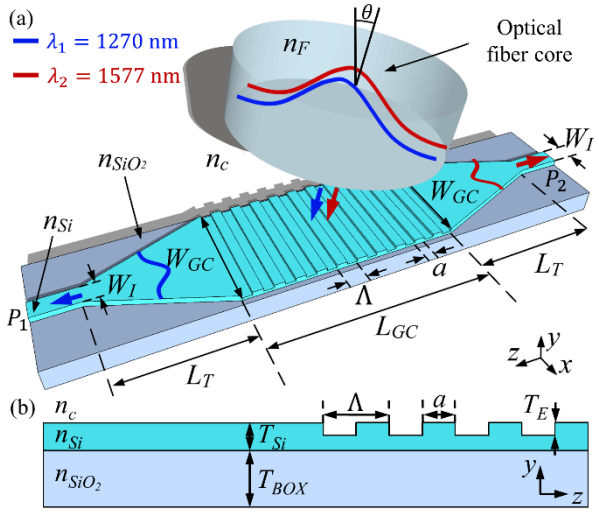

Fig. 1. (a) 3D schematic view of the dual-band fiber-chip grating coupler. The two fields that propagate through the optical fiber core at $\lambda_1 = 1270$ nm (blue curve) and $\lambda_2 = 1577$ nm (red curve) are coupled to port P_1 and P_2, respectively. (b) 2D side view of the grating coupler used during the design process.

layer. The complete device consists of two distinct parts: a taper-based spot-size converter of length L_T, and a 1D diffraction grating with a period Λ, duty cycle $DC = a/\Lambda$, and total length L_{GC}. The diffractive grating comprises unetched silicon strips (a) and shallow-etched trenches ($\Lambda - a$) with an etch depth of $T_E = 150$ nm. A cleaved single mode optical fiber (SMF-28) is positioned over the coupler with a tilt angle θ with respect to the vertical axis. The principle of operation of the coupler relies on the intrinsic change of the radiation angle with the wavelength, according to the grating equation [27]:

$$n_{FB} + p\lambda/\Lambda = n_c \sin\theta. \quad \textbf{(1)}$$

Here n_{FB} is the effective index of the fundamental Floquet-Bloch mode supported by the periodic structure, p is the diffraction order, λ is the operating wavelength, Λ is the grating period, n_c is the refractive index of the upper cladding (here, $n_c = 1$), and θ is the radiation angle. In demux configuration, the light of two different wavelengths $\lambda_1 = 1270$ nm and $\lambda_2 = 1577$ nm is coupled from the SMF-28 fiber to the chip and separated into two different waveguides, which is achieved by designing the grating to operate with opposite radiation angles for the two wavelengths. The input fields at $\lambda_1 = 1270$ nm and $\lambda_2 = 1577$ nm fulfill Eq. (1) with a positive radiation angle θ and a negative radiation angle $-\theta$, respectively. Conversely, when the coupler operates as a multiplexer, the two modes propagating in the opposite waveguides are combined and simultaneously coupled into the optical fiber. Figure 1(b) shows a side view schematic of the grating coupler. Since the width of the grating coupler (W_{GC}) is much larger than the operating wavelength, the structure can be considered as invariant in the x direction [27]. The device is designed for transverse-electric (TE) polarization. The dual-wavelength band operation of the 1D grating can be achieved by judiciously selecting the values of Λ and DC so that the radiation angle at $\lambda_1 = 1270$ nm is the opposite of that at $\lambda_2 = 1577$ nm, i.e. $\theta(\lambda_1 = 1270) = -\theta(\lambda_2 = 1577)$.

In the first step of our design, we examined both the radiation angle and the power radiated upward as a function of the grating

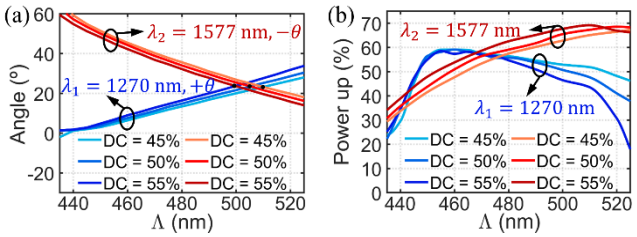

Fig. 2. (a) Radiation angle and (b) fraction of power radiated upward as a function of the grating period for different duty cycles, calculated at $\lambda_1 = 1270$ nm (blue curves) and $\lambda_2 = 1577$ nm (red curves).

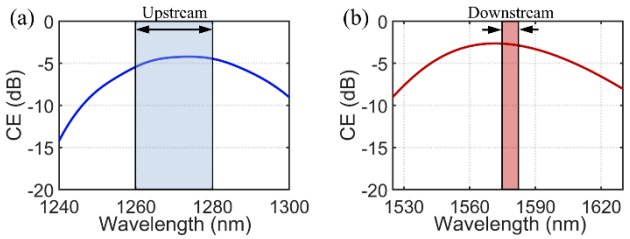

Fig. 3. Calculated coupling efficiency as a function of the wavelength near (a) $\lambda_1 = 1270$ nm and (b) $\lambda_2 = 1577$ nm.

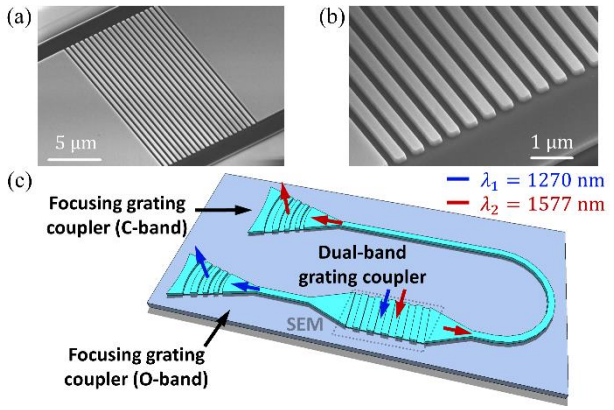

Fig. 4. (a) and (b) SEM images of the fabricated device. (c) Schematic of the test structure employed for the experimental characterization.

pitch and the duty cycle via 2D FDTD simulations (see Fig. 2). Figure 2(a) shows the absolute value of the radiation angle as a function of grating period for different duty cycles. We choose a period of $\Lambda = 500$ nm and DC = 55%, yielding the same absolute value for radiation angle for both wavelengths. In this case, the minimum feature size of the shallow-etch trench is 225 nm, thereby ensuring compatibility with 193-nm deep-UV optical lithography considered for fabrication. The width and the length of the grating were set to $W_{GC} = 17$ µm and $L_{GC} \approx 10$ µm, to maximize the overlap between the fundamental mode of the SMF-28 fiber (near-Gaussian distribution) and the radiated fields (exponential distribution). The width mismatch between the interconnection waveguides (W_I) and the grating coupler (W_{GC}) requires a spot-size converter. For this purpose, we selected linear adiabatic tapers with a length of $L_T = 500$ µm to minimize the transition loss. Figure 3 shows the calculated coupling efficiency of the coupler. The efficiency for the design wavelengths of $\lambda_1 = 1270$ nm and $\lambda_2 = 1577$ nm is as high as -4.28 dB and -2.71 dB, respectively. The simulated crosstalk is below -31 dB at $\lambda_1 = 1270$ nm and -28 dB at $\lambda_2 = 1577$ nm. In addition, the coupling efficiency spectra show a 3-dB bandwidth of 42 nm for the O-band channel, whereas the 3-dB bandwidth for the C+L channel is 75 nm. Moreover, we calculate tolerances to variations in the etch depth (T_E) and the thickness of silicon (T_{Si}) and BOX (T_{BOX}) layers. The CE penalty is 0.74 dB for $T_E \pm 10$ nm, 0.53 dB for $T_{Si} \pm 10$ nm, and 1.34 dB for $T_{BOX} \pm 200$ nm. Finally, simulations also show that a one-step antireflection stage [28] with length of 150 nm, silicon width of 200 nm and gap width of 200 nm is enough to reduce back-reflections of the proposed coupler below 3% for both 1270 nm and 1577 nm wavelengths.

The coupler was fabricated using STMicroelectronics' silicon photonics R&D and manufacturing platform based on 300-mm SOI wafers [26]. The 310-nm-thick Si layer was patterned using 193-nm deep-UV optical lithography based on a CMOS 55 nm process. A two-step etch process was used to define shallow- and full-etch trenches of the grating section and the strip waveguides. No material was deposited as upper cladding, exposing devices to air. Two different flavours with DC = 55% and DC = 50% were included in the mask. The best performance was found for the nominal design. Scanning electron microscope (SEM) images of the fabricated nominal device are shown in Figs. 4(a) and 4(b).

The experimental characterization was performed on test structures comprising a dual-band grating coupler connected to two different focusing grating couplers, each optimized for either O-band or C-band operation, as shown in Fig. 4(c). The grating trenches of the focusing couplers are described by different ellipses with common focal point between the interconnection waveguide and the grating [29]. The focusing grating coupler operating at $\lambda_1 = 1270$ nm is connected to port P_1 of our device, whereas the focusing grating coupler operating at $\lambda_1 = 1577$ nm was connected to port P_2 (see Figs. 1(a) and 4(c)). Other auxiliary test structures were also included, such as two identical focusing couplers arranged in a back-to-back configuration for both O- and C+L bands. These allowed us to determine the coupling efficiency of a single focusing grating coupler (CE_{FGC}) from the insertion loss measurements (IL_{aux}) and the setup insertion loss (IL_{setup}): $\mathrm{CE}_{FGC} = (\mathrm{IL}_{aux} - \mathrm{IL}_{setup})/2$. Note that IL_{setup} refers to the system loss for the light being transmitted through the setup in absence of the chip (i.e. no light coupling to the chip). The devices were characterized using two tunable lasers (Yenista T100S-HP-O and T100S-HP-CL), which were connected by means of a passive component tester Yenista CT400 to sweep the 1260 – 1300 nm and the 1525 – 1630 nm wavelength ranges. The light was coupled to the chip and collected from the chip using cleaved SMF-28 fibers. First, measurements of the auxiliary structures were carried out to find the optimum tilt angle of the optical fiber for the focusing grating couplers and determine their coupling efficiencies. Subsequently, the test structures were measured maintaining the optimum tilt angle for the focusing grating couplers (~17° for the coupler operating at O-band and ~7° for the coupler operating at C+L-bands). An optimum angle of $\theta \approx 21°$ was found for the fabricated dual-band grating coupler, in good agreement with our 2D FDTD simulations. The coupling efficiency of our device was determined according to: $\mathrm{CE}_{dual-band\ GC} = \mathrm{IL}_{test} - \mathrm{IL}_{setup} - \mathrm{CE}_{FGC}$, where IL_{test} is the measured insertion loss of the test structure, IL_{setup} is the setup insertion loss, and CE_{FGC} is the coupling efficiency of the corresponding focusing grating coupler. Figures 5(a) and 5(b) show the coupling efficiencies of the dual-band coupler. A coupling efficiency of -4.9 dB with a 3-dB

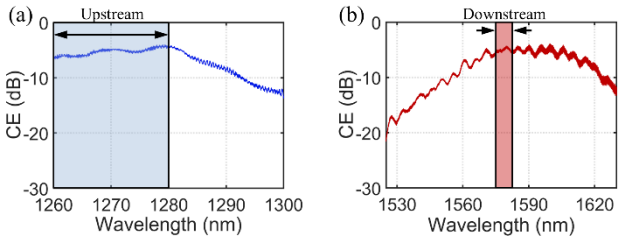

Fig. 5. Extracted coupling efficiencies near (a) $\lambda_1 = 1270$ nm and (b) $\lambda_2 = 1577$ nm.

bandwidth of 27 nm is measured at the wavelength of $\lambda_1 = 1270$ nm, limited at the lower bound by the wavelength range of our laser. Conversely, for $\lambda_2 = 1577$ nm, the coupling efficiency is as large as -5.2 dB with a 3-dB bandwidth of 56 nm. Peak coupling efficiencies of -4.3 dB and -4.6 dB were measured at the wavelengths of 1280 nm and 1600 nm, respectively. It should be noted that crosstalk is difficult to measure using this test structure due to the high rejection of the focusing grating couplers on the non-optimized bands. Ripples observed in CE measurements are due to back-reflections in the test structure. Although the contribution of our device and the focusing grating couplers to this ripple cannot be accurately separated from experimental data, larger ripples are expected in the C+L band, as the corresponding focusing grating coupler operates near the Bragg condition, with a comparatively small coupling angle of ~7°. Nevertheless, our results compare favorably to state-of-the-art dual-band couplers (see Table 1).

In summary, we report on the demonstration of a dual-band grating coupler implemented with 193-nm deep-UV lithography. The device relies on the engineering of the 1D diffractive grating to achieve opposite radiation angles, and therefore spatially separate two wavelength bands. 2D FDTD simulations show that dual-band operation is achieved with a minimal trade-off between coupling efficiency, radiation angle and fabricable design parameters. The device was fabricated using industrial-scale 300 mm silicon photonics platform. The fabricated devices show some of the highest coupling efficiencies compared to state-of-the-art dual-band grating couplers. Specifically, fiber-chip coupling efficiencies of -4.3 dB and -4.6 dB were achieved near the wavelengths of 1280 nm and 1600 nm. At XGS-PON wavelengths, the measured coupling efficiencies were -4.9 dB ($\lambda_1 = 1270$ nm) and -5.2 dB ($\lambda_2 = 1577$ nm) with a 3-dB bandwidth of 27 nm and 56 nm, respectively. The performance of the coupler could be further enhanced with apodization and also possibly achieve dual-polarization operation with the introduction of transversal subwavelength gratings [3,20]. These results prove the compatibility of our dual-band grating coupler with large-volume fabrication, paving the way towards a cost-effective deployment of efficient fiber-chip interfaces operating simultaneously in different spectral band, including applications in XGS-PON networks.

Funding. Spanish Ministry of Science, Innovation and Universities (MICINN) (RTI2018-097957-B-C33, TEC2015-71127-C2-1-R FPI scholarship BES-2016-077798); Community of Madrid - FEDER funds (S2018/NMT-4326); Horizon 2020 Research and Innovation Program (Marie Sklodowska-Curie 734331); H2020 European Research Council (ERC POPSTAR 647342); European Commission (H2020-ICT-26127-2017 COSMICC 688516); French Industry Ministry (Nano2022 project under IPCEI program); Agence Nationale de la Recherche (ANR-MIRSPEC-17-CE09-0041).

Disclosures. The authors declare no conflicts of interest.

References

1. X. Chen, M. M. Milosevic, S. Stanković, S. Reynolds, T. Domínguez-Bucio, K. Li, D. J. Thomson, F. Gardes, and G. T. Reed, Proc. IEEE **106,** 2101 (2018).
2. D. Taillaert, P. Bienstman, and R. Baets, Opt. Lett. **29,** 2749 (2004).
3. R. Marchetti, C. Lacava, L. Carroll, K. Gradkowski, and P. Minzioni, Photon. Res. **7,** 201 (2019).
4. D.-X. Xu, J. H. Schmid, G. T. Reed, G. Z. Mashanovich, D. J. Thomson, M. Nedeljkovic, X. Chen, D. Van Thourhout, S. Keyvaninia, and S. K. Selvaraja, IEEE J. Sel. Top. Quantum Electron. **20,** 189 (2014).
5. C. Kopp, S. Bernabé, B. B. Bakir, J.-M. Fedeli, R. Orobtchouk, F. Schrank, H. Porte, L. Zimmermann, and T. Tekin, IEEE J. Sel. Top. Quantum Electronics **17,** 498 (2011).
6. C. R. Doerr, L. Chen, Y.-K. Chen, and L. L. Buhl, IEEE Photon. Technol. Lett. **22,** 1461 (2010).
7. Y. Wang, W. Shi, X. Wang, Z. Lu, M. Caverley, R. Bojko, L. Chrostowski, and A. F. Jaeger, Opt. Lett. **40,** 4647 (2015).
8. A. Sánchez-Postigo, J. G. Wangüemert-Pérez, J. M. Luque-González, Í. Molina-Fernández, P. Cheben, C. A. Alonso-Ramos, R. Halir, J. H. Schmid, and A. Ortega-Moñux, Opt. Lett. **41,** 3013 (2016).
9. H. S. Abbas and M. A. Gregory, J. Netw. Comput. Appl. **67,** 53 (2016).
10. D. Zhang. D. Liu, X. Wu, and D. Nesset, J. Opt. Commun. Netw. **12,** D99 (2020).
11. C. Pinho, F. Rodrigues, A. M. Tavares, C. Rodrigues, C. E. Rodrigues, and A. Teixeira, Appl. Sci. **10,** 4024 (2020).
12. X. Guan, M. Lyu, R. Dubé-Demers, Y. Shu, W. Shi, and L. A. Rusch, in *10th Annual Information Technology, Electronics and Mobile Communication Conference (IEMCON) 2019* (IEEE,2019), p. 0920-0925.
13. Md. G. Saber, M. Osman, D. Patel, A. Samani, E. El-Fiky, M. S. Alam, K. A. Shahriar, Z. Xing, M. Jacques, B. Dortschy, G. Vall-Llosera, P. J. Urban, F. Cavaliere, S. Lessard, and D. V. Plant, Opt. Express **26,** 31222 (2018).
14. G. Roelkens, D. Van Thourhout, and R. Baets, Opt. Express **15,** 10091 (2007).
15. D. Vermeulen, G. Roelkens, J. Brouckaert, D. Van Thourhout, R. Baets, R. Duijin, E. Pluck, and G. Van den Hoven, in *34th European Conference on Optical Communication (ECOC) 2008* (IEEE,2008), p. Tu.3.C.6.
16. L. Xu, X. Chen, C. Li, and H. K. Tsang, Opt. Commun. **284,** 2242 (2011).
17. A. Y. Piggott, J. Lu, T. M. Babinec, K. G. Lagoudakis, J. Petykiewicz, and J. Vučković, Sci. Rep. **4,** 7210 (2014).
18. L. Su, R. Trivedi, N. V. Sapra, A. Y. Piggott, D. Vercruysse, and J. Vučković, Opt. Express **4,** 4023 (2018).
19. J. Tan, H. Pang, F. Meng, and J. Jiang, Chin. Phys. B **27,** 094217 (2018).
20. T. Hao, A. Sánchez-Postigo, P. Cheben, A. Ortega-Moñux, and W. N. Ye, IEEE Photon. Technol. Lett. **32,** 1163 (2020).
21. M. Streshinsky, R. Shi, A. Novack, R. T. P. Cher, A. E.-J. Lim, P. G.-Q. Lo, T. Baehr-Jones, and M. Hochberg, Opt. Express **21,** 31019 (2013).
22. W. Zhou, Z. Cheng, X. Sun, an H. K. Tsang, Opt. Lett. **43,** 2985 (2018).
23. S. Nambiar, H. Muthuganesan, T. Sharma, and S. K. Selvaraja, OSA Continuum **1,** 864 (2018).
24. L. Cheng, X. Mu, S. Wu, X. Tu, and H. Y. Fu, in *Frontiers in Optics + Laser Science APS/DLS 2019* (Optical Society of America, 2019), p. JW4A.57.
25. W. Zhou and H. K. Tsang, Opt. Lett. **44,** 3621 (2019).
26. F. Boeuf, S. Crémer, E. Temporiti, M. Ferè, M. Shaw, C. Baudot, N. Vulliet, T. Pinguet, A. Mekis, G. Masini, H. Petiton, P. Le Maitre, M. Traldi, and L. Maggi, J. Lightw. Technol. **34,** 286 (2016).
27. T. Tamir and S. T. Pend, Appl. Phys. **14,** 235 (1977).
28. D. Benedikovic, C. Alonso-Ramos, D. Pérez-Galacho, S. Guerber, V. Vakarin, G. Marcaud, X. Le Roux, E. Cassan, D. Marris-Morini, P. Cheben, F. Boeuf, C. Baudot, and L. Vivien, Opt. Lett. **42,** 3439 (2017).
29. F. Van Laere, T. Claes, J. Schrauwen, S. Scheerlinck, W. Bogaerts, D. Taillaert, L. O'Faolain, D. Van Thourhout, and R. Baets, IEEE Photon. Technol. Lett**. 19,** 1919 (2007).

Full references

1. X. Chen, M. M. Milosevic, S. Stanković, S. Reynolds, T. Domínguez-Bucio, K. Li, D. J. Thomson, F. Gardes, and G. T. Reed, "The emergenece of silicon photonics as a flexible technology platform," Proc. IEEE **106,** 2101-2116 (2018).
2. D. Taillaert, P. Bienstman, and R. Baets, "Compact efficient broadband grating coupler for silicon-on-insulator waveguides," Opt. Lett. **29,** 2749-2751 (2004).
3. R. Marchetti, C. Lacava, L. Carroll, K. Gradkowski, and P. Minzioni, "Coupling strategies for silicon photonics integrated chips," Photon. Res. **7,** 201-239 (2019).
4. D.-X. Xu, J. H. Schmid, G. T. Reed, G. Z. Mashanovich, D. J. Thomson, M. Nedeljkovic, X. Chen, D. Van Thourhout, S. Keyvaninia, and S. K. Selvaraja, "Silicon photonic integration platform – Have we found the sweet spot?," IEEE J. Sel. Top. Quantum Electron. **20,** 189-205 (2014).
5. C. Kopp, S. Bernabé, B. B. Bakir, J.-M. Fedeli, R. Orobtchouk, F. Schrank, H. Porte, L. Zimmermann, and T. Tekin, "Silicon photonic circuits: on-CMOS integration, fiber optical coupling, and packaging," IEEE J. Sel. Top. Quantum Electronics **17,** 498-509 (2011).
6. C. R. Doerr, L. Chen, Y.-K. Chen, and L. L. Buhl, "Wide bandwidth silicon nitride grating coupler," IEEE Photon. Technol. Lett. **22,** 1461-1463 (2010).
7. Y. Wang, W. Shi, X. Wang, Z. Lu, M. Caverley, R. Bojko, L. Chrostowski, and A. F. Jaeger, "Design of broadband subwavelength grating couplers with low back reflection," Opt. Lett. **40,** 4647-4650 (2015).
8. A. Sánchez-Postigo, J. G. Wangüemert-Pérez, J. M. Luque-González, Í. Molina-Fernández, P. Cheben, C. A. Alonso-Ramos, R. Halir, J. H. Schmid, and A. Ortega-Moñux, "Broadband fiber-chip zero-order surface grating coupler with 0.4 dB efficiency," Opt. Lett. **41,** 3013-3016 (2016).
9. H. S. Abbas and M. A. Gregory, "The next generation of passive optical networks: A review," J. Netw. Comput. Appl. **67,** 53-74 (2016).
10. D. Zhang. D. Liu, X. Wu, and D. Nesset, "Progress of ITU-T higher speed passive optical network (50G-PON) standardization," J. Opt. Commun. Netw. **12,** D99-D108 (2020).
11. C. Pinho, F. Rodrigues, A. M. Tavares, C. Rodrigues, C. E. Rodrigues, and A. Teixeira, "Photonic integrated circuits for NGPON2 ONU transceivers," Appl. Sci. **10,** 4024 (2020).
12. X. Guan, M. Lyu, R. Dubé-Demers, Y. Shu, W. Shi, and L. A. Rusch, "Silicon photonics for 5G passive optical networks," in *10th Annual Information Technology, Electronics and Mobile Communication Conference (IEMCON) 2019* (IEEE,2019), p. 0920-0925.
13. Md. G. Saber, M. Osman, D. Patel, A. Samani, E. El-Fiky, M. S. Alam, K. A. Shahriar, Z. Xing, M. Jacques, B. Dortschy, G. Vall-Llosera, P. J. Urban, F. Cavaliere, S. Lessard, and D. V. Plant, "Demonstration of a 120° hybrid based simplified coherent receiver on SOI for high speed PON applications," Opt. Express **26,** 31222-31232 (2018).
14. G. Roelkens, D. Van Thourhout, and R. Baets, "Silicon-on-insulator ultra-compact duplexer based on a diffractive grating structure," Opt. Express **15,** 10091-10096 (2007).
15. D. Vermeulen, G. Roelkens, J. Brouckaert, D. Van Thourhout, R. Baets, R. Duijin, E. Pluck, and G. Van den Hoven, "Silicon-on-insulator nanophotonic waveguide circuit for fiber-to-the home transceivers," in *34th European Conference on Optical Communication (ECOC) 2008* (IEEE,2008), p. Tu.3.C.6.
16. L. Xu, X. Chen, C. Li, and H. K. Tsang, "Bi-wavelength two dimensional chirped grating couplers for low cost WDM PON transceivers," Opt. Commun. **284,** 2242-2244 (2011).
17. A. Y. Piggott, J. Lu, T. M. Babinec, K. G. Lagoudakis, J. Petykiewicz, and J. Vučković, "Inverse design and implementation of a wavelength demultiplexing grating coupler," Sci. Rep. **4,** 7210 (2014).
18. L. Su, R. Trivedi, N. V. Sapra, A. Y. Piggott, D. Vercruysse, and J. Vučković, "Fully-automated optimization of grating couplers," Opt. Express **4,** 4023-4034 (2018).
19. J. Tan, H. Pang, F. Meng, and J. Jiang, "Compact and high-efficient wavelength demultiplexing coupler based on high-index dielectric nanoantennas," Chin. Phys. B **27,** 094217 (2018).
20. T. Hao, A. Sánchez-Postigo, P. Cheben, A. Ortega-Moñux, and W. N. Ye, "Dual-band polarization-independent subwavelength grating coupler for wavelength demultiplexing," IEEE Photon. Technol. Lett. **32,** 1163-1166 (2020).
21. M. Streshinsky, R. Shi, A. Novack, R. T. P. Cher, A. E.-J. Lim, P. G.-Q. Lo, T. Baehr-Jones, and M. Hochberg, "A compact bi-wavelength polarization splitting grating coupler fabricated in a 220 nm SOI platform," Opt. Express **21,** 31019-31028 (2013).
22. W. Zhou, Z. Cheng, X. Sun, an H. K. Tsang, "Tailorable dual-wavelength-band coupling in a transverse-electric-mode focusing subwavelength grating coupler," Opt. Lett. **43,** 2985-2988 (2018).
23. S. Nambiar, H. Muthuganesan, T. Sharma, and S. K. Selvaraja, "On-chip unidirectional dual-band fiber-chip grating coupler in silicon nitride," OSA Continuum **1,** 864-871 (2018).
24. L. Cheng, X. Mu, S. Wu, X. Tu, and H. Y. Fu, "Perfectly vertical grating coupler for O and C-band," in *Frontiers in Optics + Laser Science APS/DLS 2019* (Optical Society of America, 2019), p. JW4A.57.
25. W. Zhou and H. K. Tsang, "Dual-wavelength-band subwavelength grating coupler operating in the near infrared and extended shortwave infrared," Opt. Lett. **44,** 3621-3624 (2019).
26. F. Boeuf, S. Crémer, E. Temporiti, M. Ferè, M. Shaw, C. Baudot, N. Vulliet, T. Pinguet, A. Mekis, G. Masini, H. Petiton, P. Le Maitre, M. Traldi, and L. Maggi, "Silicon photonic R&D and manufacturing on 300-mm wafer platform," J. Lightw. Technol. **34,** 286-295 (2016).
27. T. Tamir and S. T. Pend, "Analysis and design of grating couplers," Appl. Phys. **14,** 235-254 (1977).
28. D. Benedikovic, C. Alonso-Ramos, D. Pérez-Galacho, S. Guerber, V. Vakarin, G. Marcaud, X. Le Roux, E. Cassan, D. Marris-Morini, P. Cheben, F. Boeuf, C. Baudot, and L. Vivien, "L-shaped fiber-chip grating couplers with high directionality and low reflectivity fabricated with deep-UV lithography," Opt. Lett. **42,** 3439-3442 (2017).
29. F. Van Laere, T. Claes, J. Schrauwen, S. Scheerlinck, W. Bogaerts, D. Taillaert, L. O'Faolain, D. Van Thourhout, and R. Baets, "Compact focusing grating couplers for silicon-on-insulator integrated circuits," IEEE Photon. Technol. Lett**. 19,** 1919-1921 (2007).